Frontiers of micro and nanomechanics of materials: Soft or amorphous matter, surface effects

Cell polarization energy and its implications for cell migration

Yuan Zhong, Shijie He, Chunying Dong, Baohua Ji *, Gengkai Hu

Biomechanics and biomaterials laboratory, School of Aerospace Engineering, Beijing Institute of Technology, Beijing 100081, China

A R T I C L E   I N F O

A B S T R A C T

Cells usually have a polarized shape in directional cell migration. This cell polarity may result from external cues, such as a gradient of chemo-attractants (chemotaxis), or a gradient of mechanical properties of substrate (durotaxis), and it can also arise from internal cues so that the cells self-polarize spontaneously and maintain the polar motile state for a long time. However, the mechanisms that control cell polarization have not been fully understood, and particularly, the relationship between the polarized shape and cell migration behaviors is not yet clear. In this study, we propose an energy model to study the cell polarization energy by considering the effect of matrix rigidity, cell shape, and organization of the cytoskeleton. We then propose a parameter called "motility factor" for depicting the relationship between the cell shape and the driving force of cell migration. We demonstrate that the fibroblast-like cell shape and keratocyte-like shape both have an optimal polarization angle corresponding to the most stable cell shape. Fibroblast-like cell shape also has an optimal tail length of the polarization. Furthermore, we find that the cell free energy biphasically depends on the matrix rigidity, i.e. that there is an optimum matrix rigidity for the most stable shape. And the motility factor also biphasically depends on the matrix rigidity, but the trends of the dependence are opposite to that of cell's free energy, which implies an optimum matrix rigidity for the highest speed. The optimum matrix rigidity for the most stable cell shape and that for the highest cell speed are consistent, suggesting that the most stable cell shape is favorable to the fastest cell migration. This study provides important insights into the relationship between cell polarization shape and cell migration behaviors.

© 2014 Académie des sciences. Published by Elsevier Masson SAS. All rights reserved.

1. Introduction

Adhesive cells often have specific polarization shapes during their directional migration. The diverse migratory behaviors of various cell types are manifested by a spectrum of their different shapes [1]. Fibroblast and keratocyte are two typical adhesive cells that were intensively studied in the past decades. In the non-polarized state, the two cells are both approximately disk-like [2–4]. But in the polarized state, fibroblasts have a spindle-like shape with a long "tail" and keratocytes have a "crescent"-like shape with two flank-like rears [1,5,6]. The transformation from the non-polarized state to the polarized one is accompanied by changes of the cell's shape and structure, such as re-organization of cytoskeleton and variation of protrusion and adhesive regions [3,7–11]. During cell polarization, the mechanical factors should play important roles in this symmetry-breaking event.

---

* Corresponding author. Tel.: +86 10 68918309.
E-mail address: bhji@bit.edu.cn (B. Ji).

Existing studies suggest that the cell may adopt a specific polarization shape for a minimum free energy. Mogilner and coworkers [12] proposed a thermodynamic model for analyzing the polarization energy of keratocytes by considering thermodynamic works by various intracellular forces. Vianay et al. [13] studied cell spreading on a protein lattice based on the principle of minimum energy, suggesting that the cell shapes were in thermodynamic metastable states. Ujihara et al. [14] simulated the change of cell shape and the cytoskeleton deformation under tensile stretching by modeling the cell as a spring network based on the minimum-energy concept. Du et al. [15] studied the effect of polymerization and depolymerization of actin filaments on cell shape and cell migration by considering the interaction between molecular motors and actin filaments as well as free energy of cell membrane. In prior studies, surface energy and volume work are the main energy components that had been considered in the modeling of different cell types [16,17].

Cell migration behaviors intensively depend on the matrix rigidity. Experiments showed a biphasic relationship between the velocity of cell migration and the rigidity of matrix [18,19]—cells migrate with low velocity on either soft or hard matrix while with a peak speed on the matrix of intermediate rigidity. The polarization shape of cells also depends on the matrix rigidity—the higher the matrix rigidity, the larger the aspect ratio of fibroblasts [3,20]. The aspect ratio of cell is defined by the ratio L_x/L_y, where L_x and L_y are the effective length and width of cell, respectively, and x is along the direction of cell migration, thus the shape of the fibroblasts is getting more spindly with increasing matrix rigidity.

To understand the cell migration behaviors, many mechanical models have been developed. Mogilner and coworkers [21] did pioneering works in modeling actin dynamics in cell migration, and also gave a comprehensive review of existing models [22]. Dokukina and Gracheva [23] developed a FEM-based model for studying the relationship between cell speed and matrix rigidity. Sarvestani [24] predicted a biphasic dependence of cell speed on matrix rigidity by considering the gradient of the density of adhesion molecules and stall force from the cell front to the cell rear. Lee et al. [25] developed a so-called "graded radial extension" (GRE) model for keratocyte by considering a graded distribution of extension and retraction rates along cell edge. Keren et al. [26] studied the role of treadmill of the actin network on the cell shape and migration based on the GRE model, and Barnhart et al. [27] further consider the effect of adhesion strength on cell shape and migration speed.

Although many efforts have been paid to either studies of cell polarization or those of cell migration, the knowledge of the relationships between the polarization shape and the migration behaviors is still lacking. The effect of matrix rigidity on cell polarization was not fully understood either. It is necessary to study the matrix-rigidity-dependent cell polarization shape and the shape-dependent cell migration behaviors for a comprehensive understanding of the relationship between cell polarization and cell migration. In this study, we first propose a thermodynamic model for cell polarization based on Mogilner's concept [12] and consider the effect of matrix rigidity on cell shape. Here we study two kinds of cells—fibroblast and keratocyte—by focusing on the fibroblast cell and by comparison of the two kinds of cells. Then we propose a parameter called "motility factor" to quantitatively describe the driving force of cell migration. At last, the relationship between cell polarization shape and cell migration behavior is discussed.

2. Models of cell polarization

2.1. The non-polarized state

For the non-polarized state, both fibroblast and keratocyte have disk-like cell shape [2,3,8,12] (Fig. 1). The actin filament and myosin are assumed to be distributed homogeneously in the cell based on experimental observations [2]. Most of actin filament networks near the cell membrane make isotropic polymerization, producing an isotropic protrusion force. The total protrusion force is assumed to be constant [12]. Generally, cytoplasmic pressure σ_{mem} applied on the cell membrane is isotropic in the cell membrane plane. The actin filament bundle distributed at the cell's periphery may form by cytoplasmic retraction or centripetal cytoplasmic flow [28,29]. The initial radius of the cell before polarization is R_0. The cells without polarization have a free energy E_0 that is called the initial free energy.

2.2. The polarized state

The transformation of a cell from the non-polarized state to the polarized one is produced by the intracellular forces. Before polarization, the actin filament network near the cell membrane provokes an isotropic polymerization, producing an isotropic protrusion force. In the polarization process, while polymerization is kept at the cell front, that at the cell rear stops, replaced by depolymerization [8]. Thus, the equilibrium of the cell membrane breaks, and a concave cell shape forms at the cell rear with the cytoplasmic retraction or centripetal cytoplasmic flow [29].

For a clear description in the model, we use superscript "f" for the variables and parameters of fibroblast and "k" for those of keratocyte, and those without superscript are applied to both cells.

For fibroblast, the cell shows an arc-like convex front edge and a characteristic long tail at the cell rear [1]. This typical shape can be described by the polarization angle φ^f, radius of cell front R^f and length of cell tail L^f (see Fig. 1 & 2). In our model, the protrusion force at the cell front is considered as constant for the expansion of the cell leading edge, while the protrusion force at the cell rear concentrates at the endpoint and helps the formation of the cell tail. At the cell periphery, the surface tension λ_B^f is generated by the contractile myosin of the actin filament bundle, keeping the concave shape at the cell rear under pressure σ_{mem} [16,28]. The actin filaments are re-oriented to align along the migrating direction of
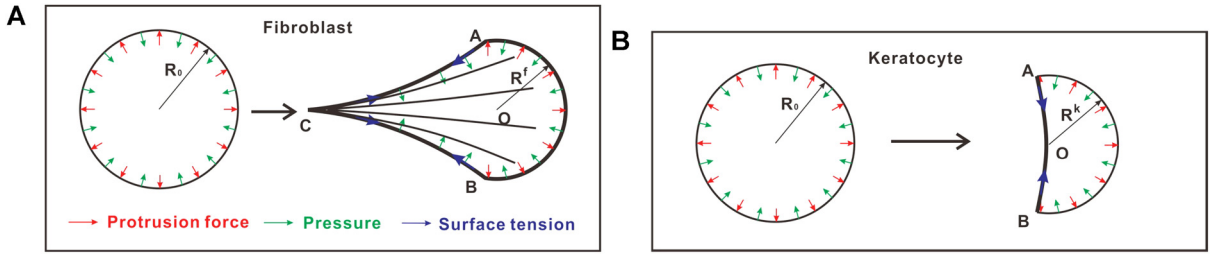
Fig. 1. Schematic illustration of the polarization of a fibroblast and of a keratocyte. A) Evolution of the fibroblast cell from a disc-like shape to a spindly shape with distinct re-organization of the cytoskeleton under the intracellular forces—the protrusion force generated by actin filament polymerization (shown as red arrow) and the pressure on the cell membrane (shown as a green arrow), tension force of the actin filament bundle (shown as a blue arrow). B) The evolution of the keratocyte cell from a disc-like shape to a crescent-like one under intracellular forces. (For interpretation of references to color in this figure, the reader is referred to the web version of this article.)

the cell. During the polarization of the fibroblast, it is observed in experiments that actin filaments depolymerize at the cell rear, except the endpoint of the tail [8] which instead exhibits protrusion [30].

For the keratocyte, Mogilner [12] showed a crescent shape with the polarization angle φ^k and radius of cell front R^k. It is hypothesized that for a symmetry-breaking polymerization under mechanical disturbance, the isotropic actin network is collapsed into the rear edge. At the opposite side, referred to as the front edge, actin filaments keep polymerizing and, hence, pushing on the membrane. The surface tension in actin filament bundle at the cell rear, resulting from the additive action of the condensed myosin molecules, is equal to the contractile stress in the actin-myosin ring multiplied by the width of the ring $\lambda_B^k = \gamma_{net}^k \frac{R_0}{2}$.

2.3. Free energy of the polarized cell

2.3.1. Fibroblast

The protrusion force generated by the polymerization of the actin filament network will cause the extension of the cell edge in the normal direction. At the cell front, the protrusion force is $F_f^f = F^f \cdot \frac{2\pi - \varphi^f}{2\pi}$. At the cell rear, the protrusion force converges on the endpoint of the cell tail (point C in Fig. 1), causing a relative backward movement. Thus, the effective protrusion force is $F_r^f = \int_{-\frac{\varphi^f}{2}}^{\frac{\varphi^f}{2}} \frac{F^f}{2\pi} \cos \varphi' \, d\varphi'$.

The protrusion force induces the decrease of potential energy by:

$$E_1^f = -\left(\int F_f^f \, dR^f + \int F_r^f \, dL^f \right) \tag{1}$$

where R^f is the radius of the cell front.

The actin filament cytoskeleton will reorganize into elongated actin filament bundles (stress fibers) parallel to the polarization direction. Generally, the pre-strain of a stress fiber is approximately 0.1 according to experimental observations, i.e. $\varepsilon_s^f = 0.1$ [31–33]. Thus, the tension force is $F_s^f = E_s^f A_s^f \varepsilon_s^f \approx 4.5$ nN, where E_s^f and A_s^f are Young's modulus and the cross-section area of the stress fiber, respectively [34,35]. The total number of stress fibers N_s^f is assumed to be constant. In this study, we chose $N_s^f = 10$, a value that is consistent with the experimental measurements [36]. Therefore, the strain energy of the parallel actin filament bundles is:

$$E_2^f = \int \frac{1}{2} N_s^f F_s^f \varepsilon_s^f \, dL_{s0}^f \tag{2}$$

where L_{s0}^f is the length of the stress fibers.

The surface energy (in the 2D model) induced by the surface tension at the cell's periphery is:

$$E_3^f = \int \lambda_B^f \, dL_B^f \tag{3}$$

where L_B^f is the total length of the actin filament bundles along the cell edge.

The intrinsic volume (area in 2D model) energy affected by the pressure is

$$E_4^f = \int \sigma_{mem}^f \, dA^f \tag{4}$$

Both the surface energy and the intrinsic volume energy are usually considered in the modeling of adhesive and spreading cells [16,17,37].
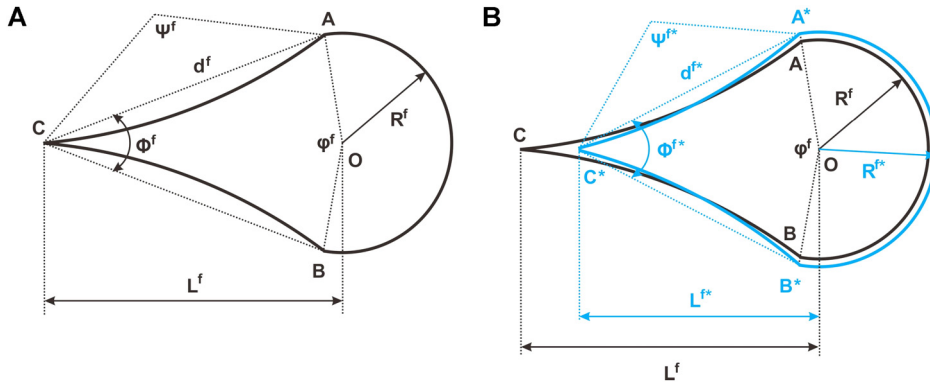
Fig. 2. Illustration of the cell polarization shape and corresponding shape parameters of the fibroblast (rigidity and elastic matrix). A) Rigid matrix; B) elastic matrix—the blue line stands for the cell shape on the elastic matrix case, while the black line stands for the cell shape on the rigid matrix one for comparison. The notations of parameters are also written in corresponding colors. (For interpretation of references to color in this figure, the reader is referred to the web version of this article.)

Here we also consider the interaction energy between the cell and the matrix at the focal adhesion complexes (FACs) in which the matrix stiffnesses play important roles. For instance, the aspect ratio of the fibroblast on the stiffer matrix is much larger than that on the softer one [3,20]. Here the rigidity of the matrix is considered by the effective spring constant k_m, which can be estimated by $k_m = \frac{2aE_m}{1-v_m^2}$ [38,39], where a is the size of FAC, and E_m and v_m are Young's modulus and Poisson's ratio of the matrix, respectively. The cell adhesion in the region of lamellipodia at the cell front [3] (AB arc in Fig. 2) is considered as continuous small adhesion, with force density $\vec{f}_{ad}$. The adhesions at the flanks of the cell (points A and B in Fig. 2) and the endpoint of cell tail (point C in Fig. 2) are considered as discrete large adhesions. The cell–matrix interaction energy is then written as:

$$E_5^f = -\left(\iint f_{ad}\,dl\,dR^f + \sum_i \int F_{FA,i}^f\,dR^f + \int F_{FA,3}^f\,dL^f \right) \tag{5}$$

where $i = 1$ and $i = 2$ indicate points A and B in Fig. 2, respectively; the subscript '3' of $F_{FA,3}^f$ indicates point C. The expression of continuous adhesion energy is consistent with that in [17]. $F_{FA,1}^f = F_{FA,2}^f = k_m\Delta R$ ($\Delta R = \overline{AA^*} = \overline{BB^*}$) are the traction forces of focal adhesions at the two flanks of the cell rear, and $F_{FA,3}^f = k_m\overline{CC^*} = k_m\Delta L$ at the cell rear (see Fig. 2B).

The total change of the free energy of the cell is:

$$E_{tot}^f = E_1^f + E_2^f + E_3^f + E_4^f + E_5^f - E_0 \tag{6}$$

where E_0 is the initial energy of the cell before cell polarization. The first four terms do not depend on the rigidity of the matrix, but the fifth term does.

Before calculating the free energy, we first analyze the cell geometry on a rigid matrix. The cell shape of the fibroblast on a rigid matrix is shown in Fig. 2A. We assume that the area of the cell is constant during polarization according to experimental observations [3,40], thus $E_4^f = 0$. Considering the constant cell area and the geometrical relationship, we have:

$$\begin{cases} \pi(R_0)^2 = \frac{2\pi - \varphi^f}{2}(R^f)^2 + L^f \cdot R^f \sin\left(\frac{\varphi^f}{2}\right) - (\rho^f)^2(\Psi^f - \sin\Psi^f) \\[2mm] \Psi^f = 2\arcsin\left(\frac{d^f}{2\rho^f}\right) \\[2mm] d^f = \sqrt{\left[L^f - R^f\cos\frac{\varphi^f}{2}\right]^2 + (R^f)^2\sin^2\frac{\varphi^f}{2}} \end{cases} \tag{7}$$

where ρ^f is the radius of arc AC and BC at the cell rear (see Fig. 2). According to the Laplace equation [16,17,37] (see Fig. 2), we have:

$$\rho^f = \frac{\lambda_B^f}{\sigma_{mem}} \tag{8}$$

Given the values of R_0 and φ^f, we can calculate d^f, Ψ^f and R^f. This nonlinear system of equations can be solved by using the Newton–Raphson method. Then we can calculate the free energy of the cell on the rigid substrate.

To calculate the cell geometry on the elastic matrix, we should first consider the equilibrium of adhesion forces at the cell front as:
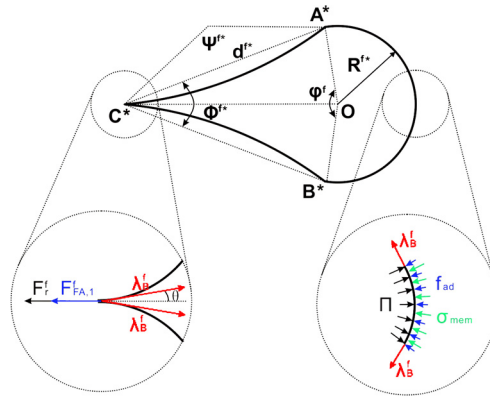
Fig. 3. (Color online.) Illustration of the equilibrium of cell adhesions at the cell front and at the end point C* of the cell rear of a fibroblast.

$$\vec{f}_{ad} + \left(\frac{\lambda_B^f}{R^{f*}} + \sigma_{mem}\right)\vec{n} + \frac{d\vec{F}_f^f}{dL_{front}^{f*}} = \vec{0} \tag{9}$$

which is shown in Fig. 3, where f_{ad} is the adhesion force at the cell front, R^{f*} is the new radius of the cell front because of the deformation of the elastic deformation under the traction force. L_{front}^{f*} is the length of the cell front, given by $L_{front}^{f*} = (2\pi - \varphi^{f*})R^{f*}$. The first three terms are consistent with those in Bischofs' model [17]. The fourth term is the protrusion force, consistent with that in Mogilner's model [12]. The pressure is assumed to be constant in our model as $\sigma_{mem} = 0.1$ nN/μm [36,41].

Also considering the equilibrium of point C* at the cell tail (see Fig. 3), we have:

$$\vec{F}_\lambda^f + \vec{F}_r^f + \vec{F}_{FA,3}^f = \vec{0} \tag{10}$$

where

$$F_\lambda^f = 2\lambda_B^f \cos\theta \tag{11}$$

and $\theta = \frac{\Phi^{f*}}{2} - \frac{\Psi^{f*}}{2}$ is the angle between the direction of surface tension and line OC*, Φ^{f*} is the angle of line A*C* and B*C*, $\Phi^{f*} = 2\arcsin(\frac{R^{f*}}{d^{f*}}\sin\frac{\varphi^{f*}}{2})$, and Ψ^{f*} is the central angle of arc A*C* or B*C*, as shown in Fig. 2B.

F_r^f is the effective protrusion force. The relationship between the adhesion force and the effective stiffness of the matrix is:

$$F_{FA,3}^f = k_m(L^f - L^{f*}) \tag{12}$$

where L^f and L^{f*} are the lengths of the tail on the rigid and elastic matrices, respectively; k_m is the effective stiffness of the elastic matrix.

Considering the geometrical relationship and the constant cell area condition, we get the following system of equations as

$$\begin{cases} \pi(R_0)^2 = \frac{2\pi - \varphi^f}{2}(R^{f*})^2 + L^{f*}R^{f*}\sin\left(\frac{\varphi^f}{2}\right) - (\rho^{f*})^2(\Psi^{f*} - \sin\Psi^{f*}) \\ \\ \Psi^{f*} = 2\arcsin\left(\frac{d^{f*}}{2\rho^{f*}}\right) \\ \\ d^{f*} = \sqrt{\left(L^{f*} - R^{f*}\cos\frac{\varphi^f}{2}\right)^2 + (R^{f*})^2\sin^2\frac{\varphi^f}{2}} \end{cases} \tag{13a}$$

$$\Phi^{f*} = 2\arcsin\left(\frac{R^{f*}}{d^{f*}}\sin\frac{\varphi^f}{2}\right) \tag{13b}$$

$$k_m(L^f - L^{f*}) = 2\lambda_B^f\cos\left(\frac{\Phi^{f*}}{2} - \frac{\Psi^{f*}}{2}\right) - F_r^f \tag{13c}$$

where $\rho^{f*} = \rho^f = \lambda_B^f/\sigma_{mem}$. Compared with Eq. (7), there are two addition equations in Eq. (13), i.e. (13b) for the angle Φ^{f*}, and (13c) is for the equilibrium of FAC at point C*. Again, the nonlinear system of equations can be solved by using the Newton–Raphson iteration method. Thus, we can calculate the free energy of the cell at the elastic substrate. (The values of main parameters are given in Table 1.)

Table 1
Main parameters.

| Parameters	Symbol	Value	References
Total protrusion force of a fibroblast	F^f	100 nN	[62]
Total protrusion force of a keratocyte	F^k	6 nN	[12]
Surface tension of a fibroblast	λ_B^f	20 nN	[36]
Surface tension of a keratocyte	λ_B^k	1.5 nN	[12]
Pressure	σ_{mem}	0.1 nN/μm	[36,41]
Young's modulus of a stress fiber	E_s^f	1.45 μN/μm^2	[34,35]
Cross section area of a stress fiber	A_s^f	3.14×10^{-2} μm^2	[34,35]
Pre-strain of a stress fiber	ε_s^f	0.1	[31]
Homeostatic stress of FA	σ	5.0 kPa	[46–48]
Young's modulus of the matrix	E_m	1–100 kPa	[63,64]
Fitting parameter in Eq. (27)	A_{FA}^{max}	6 μm^2	[57]
Fitting parameter in Eq. (27)	β	0.2	[57]
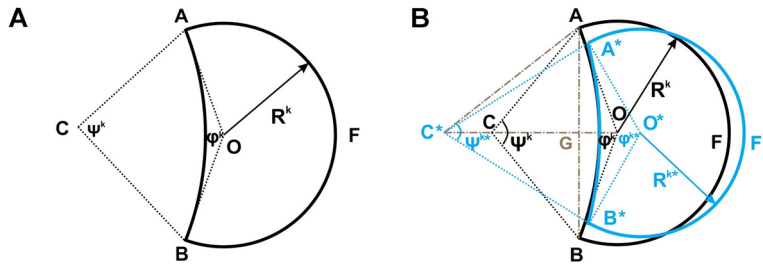
Fig. 4. Illustration of the cell polarization shape and corresponding shape parameters of keratocyte (rigidity and elastic matrix). A) Rigid matrix; B) elastic matrix—the blue line stands for the cell shape on the elastic matrix case, while the black one stands for the cell shape in the rigid matrix one for comparison. (For interpretation of references to color in this figure, the reader is referred to the web version of this article.)

2.3.2. Keratocyte

Different from the fibroblast, here all the protrusion forces are applied to the cell front, the decrease of potential energy by protrusion is [12]:

$$E_1^k = - \int F^k \, dR \tag{14}$$

The energy change caused by the contraction of actin–myosin network is:

$$E_2^k = \int \gamma_{net}^k \, dA_{net}^k \tag{15}$$

where $A_{net}^k = \frac{3}{8}(2\pi - \varphi^k)(R_0)^2$ is the area of actin–myosin network region.

The surface energy (in the 2D model) induced by the surface tension of the peripheral actin filament bundle at cell rear is:

$$E_3^k = \int \lambda_B^k \, dL_B^k \tag{16}$$

where L_B^k is the arc length of the concave actin filament bundle AB at the cell rear (Fig. 4), which is different from the fibroblast.

Similar to the fibroblast, the change of the intrinsic volume (area in 2D model) energy by the pressure is:

$$E_4^k = \int \sigma_{mem} \, dA^k \tag{17}$$

Finally, we consider the interaction energy between the cell and the matrix. Similar to the fibroblast, the cell adhesion at the cell front (arc AFB in Fig. 4) is considered as a continuous adhesion with force density f_{ad}. The cell adhesions at the two "pincher"-like flanks of the cell rear (points A and B in Fig. 4) are considered as discrete adhesions with forces $F_{FA,1}^k$ and $F_{FA,2}^k$. Similar to the energy terms of the fibroblast, the free energy change because of the matrix rigidity is:

$$E_5^k = -\left(\iint f_{ad} \, dl \, dR^k + \sum_i \int F_{FA,i}^k \, d\varsigma_i^k \right) \tag{18}$$

where $F_{FA,1}^k = k_m \varsigma_1^k$ and $F_{FA,2}^k = k_m \varsigma_2^k$ are the traction forces at the discrete focal adhesions at the two cell rears, and $\varsigma_1^k = \overline{AA^*}$ and $\varsigma_2^k = \overline{BB^*}$ are the displacement of substrate of points A and B, respectively (Fig. 4B).

The total change of free energy is:

$$E_{tot}^k = E_1^k + E_2^k + E_3^k + E_4^k + E_5^k - E_0 \tag{19}$$

Consistent with the fibroblast's case, only the fifth term depends on matrix stiffness.

On a rigid matrix, the parameters of the shape of keratocyte are given by [12]:

$$\Psi^k = 2\arcsin\left(\frac{F^k}{\lambda_B^k} \frac{\sin(\varphi^k/2)}{2\pi - \varphi^k}\right) \tag{20}$$

$$R^k = \frac{R_0}{\sqrt{1 - \frac{1}{2\pi}(\varphi^k - \sin\varphi^k) - \frac{1}{2\pi}(\frac{\lambda_B^k}{F^k})^2(2\pi - \varphi^k)^2(\Psi^k - \sin\Psi^k)}} \tag{21}$$

in which the relation

$$\rho^k = \frac{\lambda_B^k}{\sigma_{mem}} = \frac{\lambda_B^k}{F^k} \cdot (2\pi - \varphi^k) \cdot R^k \tag{22}$$

has been applied, where ρ^k is the radius of arc AB at the cell rear, as shown in Fig. 4. The nonlinear system of equations (Eqs. (20) and (21)) for a rigid matrix can be solved by using the Newton–Raphson iteration method.

On an elastic matrix, we consider the effect of matrix stiffness on the cell polarization shape and the corresponding free energy. Before calculating the deformation energy at focal adhesion (Eq. (18)), we first consider the force equilibrium at focal adhesion. Because a keratocyte cell front is similar to that of a fibroblast, Eq. (9) is also applied to the keratocyte at the cell front. For a keratocyte, the surface tension at the cell front λ_f^k is primarily generated by the cell membrane due to the lack of actin filament bundle [4,11], and the bending modulus of the cell membrane is as low as 10^{-19} J [42]; therefore the influence of surface tension λ_f^k is negligible. In addition, because the cell adhesion at the cell front of a keratocyte is highly dynamic and unstable [43], the influence of cell adhesion is also negligible, i.e. $f_{ad} \approx 0$. Thus, at the cell front, we have $\sigma_{mem} = \frac{dF^k}{dL_f^k}$.

For the equilibrium at the large focal adhesion at the cell rear A and B, the traction force at the focal adhesion is equal to the tension of the bundle λ_B^k, i.e. $\lambda_B^k = k_m \overline{AA^*} = k_m \overline{BB^*}$; therefore we have:

$$\frac{\lambda_B^k}{k_m} = \sqrt{\left(x_0^{k*} - R^{k*}\cos\frac{\varphi^{k*}}{2} + R^k\cos\frac{\varphi^k}{2}\right)^2 + \left(R^{k*}\sin\frac{\varphi^{k*}}{2} - R^k\sin\frac{\varphi^k}{2}\right)^2} \tag{23a}$$

where $x_0^{k*} - R^{k*}\cos\frac{\varphi^{k*}}{2} + R^k\cos\frac{\varphi^k}{2}$ and $R^{k*}\sin\frac{\varphi^{k*}}{2} - R^k\sin\frac{\varphi^k}{2}$ are x and y components of $\overline{AA^*}$ (or $\overline{BB^*}$), respectively, and $x_0^{k*} = \overline{OO^*}$.

Similar to the case of rigid matrix, the geometrical relationship and constraint of the constant cell area are given as:

$$\begin{cases} \Psi^{k*} = 2\arcsin\left(\frac{F^k}{\lambda_B^k} \cdot \frac{\sin(\varphi^{k*}/2)}{2\pi - \varphi^{k*}}\right) \\ R^{k*} = \frac{R_0}{\sqrt{1 - \frac{\varphi^{k*} - \sin\varphi^{k*}}{2\pi} - \frac{1}{2\pi}(\frac{\lambda_B^k}{F^k})^2(2\pi - \varphi^{k*})^2(\Psi^{k*} - \sin\Psi^{k*})}} \\ \rho^{k*} = \frac{\lambda_B^k}{F^k} \cdot (2\pi - \varphi^{k*}) \cdot R^{k*} = \frac{\lambda_B^k}{\sigma_{mem}} \end{cases} \tag{23b}$$

They correspond to Eqs. (20)–(22) for the case of a rigid matrix. If we consider the geometry relation $\overline{AC^{*2}} = \overline{AA^{*2}} + \overline{A^*C^{*2}} = \overline{AG^2} + \overline{GC^{*2}}$, we further have:

$$\left(\frac{\lambda_B^k}{k_m}\right)^2 + (\rho^{k*})^2 = \left(\rho^{k*}\cos\frac{\Psi^{k*}}{2} - \left(x_0^{k*} - R^{k*}\cos\frac{\varphi^{k*}}{2} + R^k\cos\frac{\varphi^k}{2}\right)\right)^2 + \left(R^k\sin\frac{\varphi^k}{2}\right)^2 \tag{23c}$$

The nonlinear system of equations (Eqs. (23a)–(23c)) can be solved by using the Newton–Raphson iteration method. Thus, we can calculate the total change of free energy of the cell polarization of a keratocyte using Eq. (19).
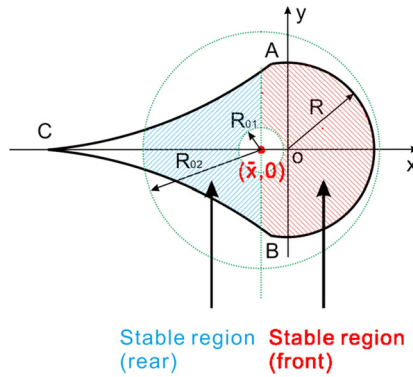
Fig. 5. Illustration of the stable region of cell adhesion defined by R_{01} and R_{02} in Eq. (29). The area with hatched lines shows the stable region of cell adhesion. The areas with a red hatched line and that with a blue line correspond to the stable region of the cell front and cell rear, respectively. (For interpretation of references to color in this figure, the reader is referred to the web version of this article.)

3. The motility factor

The adhesions at the cell front generate a propulsive traction force while those at the cell rear generate a resistance force against cell migration [6,44]. Before the detachment of the cell rear, the total adhesion forces (traction force) are in equilibrium. Increasing evidences show that the cell might use its shape to control the dynamics of adhesion at the cell front and the cell rear, e.g., by breaking the balance of adhesion between the cell front and the cell rear, and thus to produce the driving force for cell migration [45]. Here we propose a parameter that quantitatively depicts the magnitude of the driving force.

The traction force on a single focal adhesion complex (FAC) can be written as:

$$F = \sigma A_{\text{FA}} \tag{24}$$

where σ and A_{FA} are the mean traction stress and the area of focal adhesion, respectively. The mean traction stress of focal adhesion is assumed to be constant [46–48]. Experimental and theoretical studies [49] showed that there is an approximately linear relationship between local traction forces and the distance from the cell centroid, thus there is $A_{\text{FA}} = \xi l_c$, where ξ is the gradient of focal adhesion area, l_c is the distance from the cell centroid $l_c = \sqrt{(x - \bar{x})^2 + (y - \bar{y})^2}$, and $(\bar{x}, \bar{y})$ are the coordinate of the cell centroid [50]. Experiments demonstrated that there is a linear relationship between the area of focal adhesion and the distance from the cell centroid [51,52]. Thus, the traction force is [53]:

$$F_x = \sigma \xi (x - \bar{x})$$
$$F_y = \sigma \xi (y - \bar{y}) \tag{25}$$

To gain a quantitative understanding of how cell shape influences cell migration behaviors, we defined a parameter called "motility factor" as [50]:

$$\Gamma = \left. \frac{\int_{A_{\text{cell front}}} \sigma \xi (x - \bar{x}) \, dA}{\int_{A_{\text{cell rear}}} \sigma \xi (x - \bar{x}) \, dA} \right|_c \tag{26}$$

Here we set that the cell migrates along the x axis, which is also the axis of symmetry of the cell, as shown in Fig. 5. We see that the motility factor is the ratio of the propulsive traction force at the cell front to the resistant traction force at the cell rear at the critical condition of detaching the cell rear. In Eq. (26), the "cell front" indicates the region where $x > \bar{x}$, while the "cell rear" indicates the one where $x < \bar{x}$. The larger the value of the "motility factor", the higher the driving force for cell migration.

To determine the critical condition of detachment of the cell rear, we first calculate the stability of FACs. The state of the FACs is closely associated with the applied force [54,55], which has a stabilizing to disruptive transition with increasing cell traction, i.e. from nascent FACs to mature FACs and then to disassembled adhesions. The typical size of nascent FACs is on the order of 1 μm² [48], and the stress on it is about 1 kPa [56,57]. If we adopt a minimum area of FACs of 1 μm², we obtain the lower limiting value of the traction force F_{01} as 1 nN. The upper limiting value F_{02} can be calculated as $F_{02} = \sigma A_{\text{FA}}^*$, where A_{FA}^* is the maximum area of FACs. According to experiments, we assume the maximum area of FACs depends on the rigidity of matrix, which can be formulated by fitting experimental data [57] as:

$$A_{\text{FA}}^* = A_{\text{FA}}^{\max} \left(1 - e^{\beta E_m} \right) \tag{27}$$

Once the values of F_{01} and F_{02} are determined, the stable region of cell adhesions is given by the inequality as
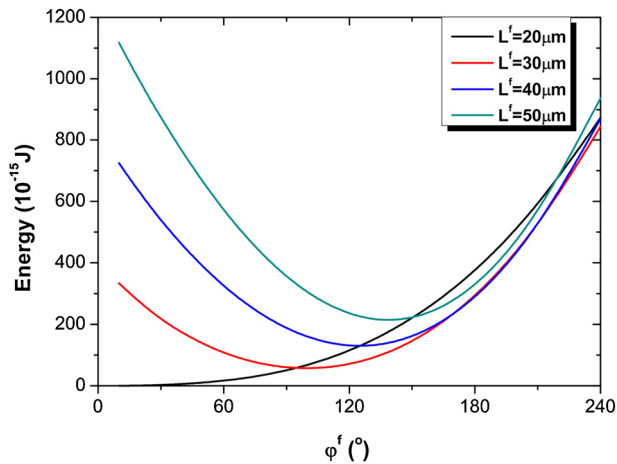
Fig. 6. (Color online.) Relationship between the free energy and the polarization angle of a fibroblast. There is a biphasic relationship between the free energy and the polarization angle. The longer the cell tail, the larger the optimal polarization angle.
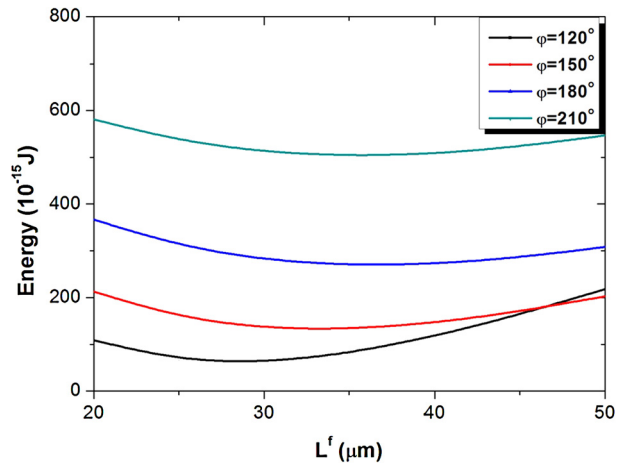
Fig. 7. (Color online.) Relationship between the free energy and the tail length of the fibroblast. There is a biphasic relationship between the free energy and the tail length.

$$F_{01} \leqslant F \leqslant F_{02} \tag{28}$$

which defines a ring-shape area $R_{01} \leqslant l_c \leqslant R_{02}$ as shown in Fig. 5, where the two radii R_{01} and R_{02} are given by:

$$\begin{cases} R_{01} = \dfrac{F_{01}}{\sigma \xi} \\ R_{02} = \dfrac{F_{02}}{\sigma \xi} \end{cases} \tag{29}$$

Note that F_{02} is a function of the rigidity of matrix; thus the area with stable adhesion at the cell front and rear is determined by the matrix rigidity and the cell shape.

4. Results

4.1. Effect of the polarization angle on cell free energy

The effect of the polarization angle on cell free energy of the fibroblast is shown in Fig. 6. For different tail lengths L^f, there is a minimum free energy value corresponding to an optimal polarization angle for a stable migration state. When the tail length is equal to the initial radius $R_0 = 20$ μm, the corresponding polarization angle is zero, reproducing the non-polarized state of the cell and suggesting that it is also a metastable state. We see that the optimal angle increases with the tail length. Mogilner et al. [12] showed that there is also an optimal polarization angle for a keratocyte, corresponding to its stable migration state.

We note that for both fibroblast and keratocyte, there is a biphasic relationship between cell free energy and polarization angle, and the minimum of free energy corresponds to a stable state of the polarized cells. The difference between fibroblast and keratocyte is that the free energy of the fibroblast is not only dependent on the polarization angle, but also on the tail length.

4.2. Effect of the tail length of the fibroblast

Fig. 7 shows the influence of the tail length on the cell's free energy. There is also a biphasic relationship between the tail length and the cell's free energy with various polarization angles, suggesting an optimal tail length for a stable polarization state of the fibroblast. This relationship implies that the growth of the cell tail is limited by the geometric evolution of the cell toward a minimum cell free-energy value, i.e. the cell tends to change its shape for an optimal tail length with minimum energy. The cell energy is also related to the cell adhesion at the cell tail, e.g., experiments showed that the cell tail retracts during cell migration [6], which is expected to be related to de-adhesion of the cell rear. The biphasic relationship between tail length and cell energy implies that the characteristic shape of the fibroblast changes during its migration.

4.3. Effect of matrix rigidity on cell energy and motility factor

Fig. 8 shows the effect of matrix rigidity on the cell free energy and on the cell motility factor of the fibroblast for different tail lengths. We found that both cell free energy and motility factor are biphasically dependent on the rigidity of matrix, but the trends of their dependence are opposite. On the soft matrix, the cell has high free energy and low motility factor. With increasing matrix rigidity, the cell energy decreases while the motility factor increases, approaching a minimum energy and a maximum motility factor at an optimal matrix rigidity, respectively. When the matrix rigidity becomes larger than the optimal rigidity, the cell has high energy and low motility
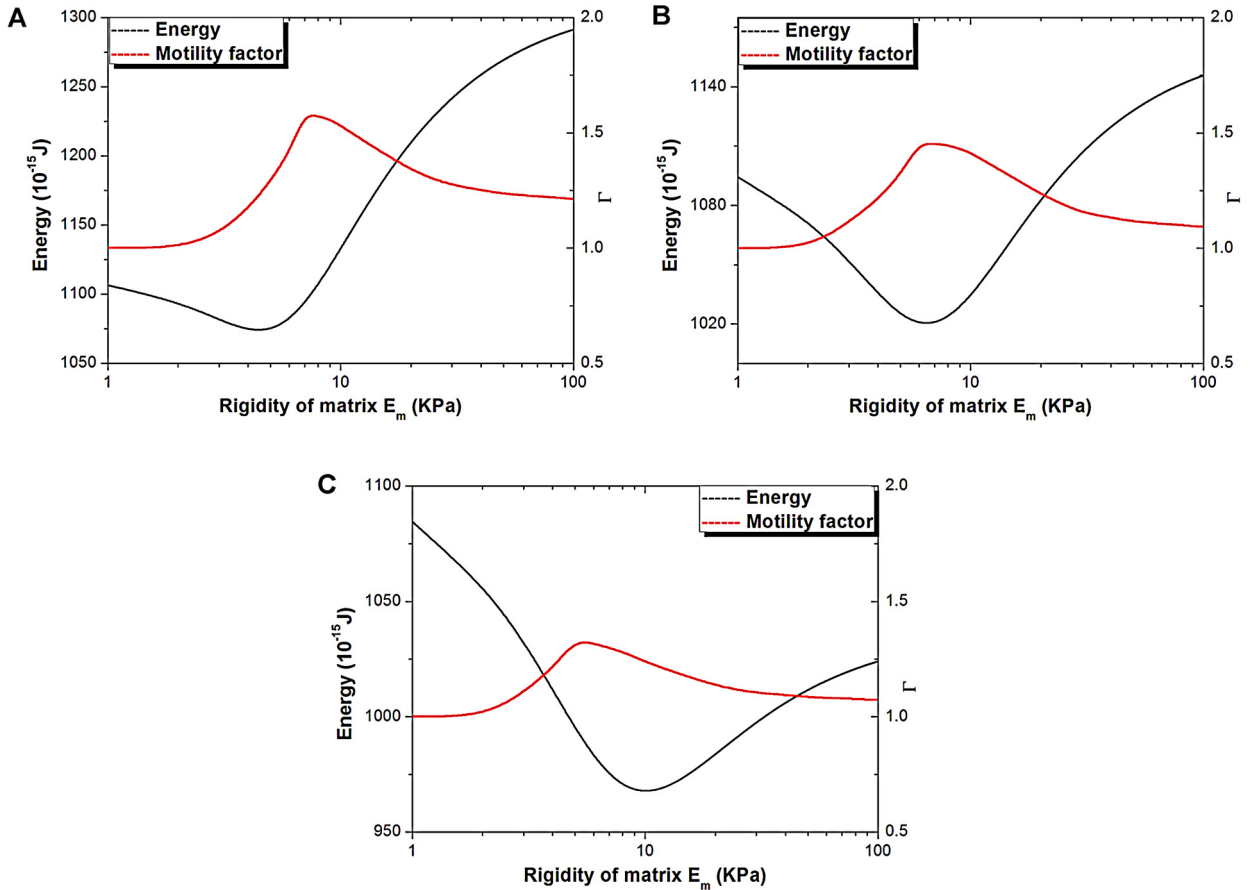
Fig. 8. (Color online.) Dependence of the free energy and the motility factor of a fibroblast upon matrix rigidity for different tail lengths. A) $L_m = 80$ μm; B) $L_m = 70$ μm; C) $L_m = 60$ μm. There is a biphasic relationship between free energy and matrix rigidity; the trend is opposite to that of the relationship between motility factor and matrix rigidity. The value of the optimal matrix rigidity for the minimum cell energy is close to that for the maximum motility factor.

factor again. It is interesting to note that the value of optimal matrix rigidity for the minimum cell energy is roughly equal to that for the maximum motility factor. This result suggests that the cell geometry with minimum free energy is also optimized for the production of a maximum driving force for cell migration.

The biphasic relationship between the motility factor and the rigidity of the matrix is consistent with the biphasic relationship between the cell migration speed and the rigidity of matrix found in experiments [18–20]. The biphasic relationship between cell energy and matrix rigidity implies that the cell polarization regulated by the matrix rigidity adopts the principle of energy minimization [3,20].

A keratocyte exhibits similar biphasic behaviors regarding the relationship between cell energy and matrix rigidity and that between motility factor and matrix rigidity, as shown in Fig. 9. Similarly, the value of the optimal matrix rigidity for a minimum cell energy is close to that for a maximum motility factor.

4.4. Effect of cell shape on the motility factor

Fig. 10 shows the comparison of motility factors between fibroblast and keratocyte with different matrix rigidities. The tail length of the fibroblast is set as $L_m^f = 80$ μm. Both motility factors show a biphasic dependence on matrix rigidity for the two cell shapes. The motility factor of the keratocyte is larger than that of the fibroblast for different matrix rigidities. For the optimal rigidity, the motility factor of the keratocyte is two times larger than that of the fibroblast. Because the motility factor represents the driving force and the efficiency of cell migration, our result is consistent with the experimental results evidencing that the cell speed of the keratocytes is much higher than that of fibroblasts [5,58]. The mechanism is that the "pincers"-like cell rears of the keratocyte can produce a larger detachment area than those of the fibroblast for producing the driving force.

5. Discussion

In this study, we analyzed the free energy of cell polarization and its dependence on matrix rigidity and cell types. We showed that the cell free energy depends on the active protrusion of cell periphery, the active contractility of the cytoskeleton, the structure and organization of the cytoskeleton, and the mechanics of cell–matrix interaction mediated by
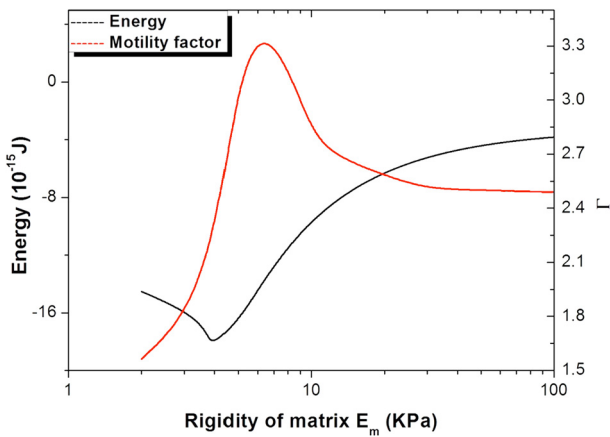
Fig. 9. (Color online.) Dependence of the free energy and the motility factor of a keratocyte upon matrix rigidity. Similar to the fibroblast, the value of the optimal matrix rigidity for the minimum cell energy is close to that for the maximum motility factor.
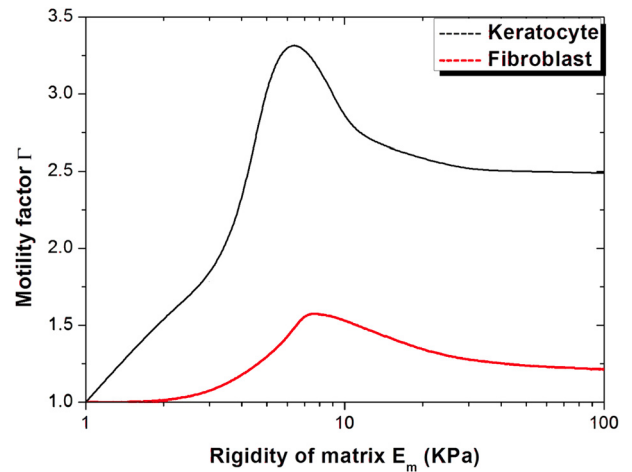
Fig. 10. (Color online.) Comparison of motility factor values between fibroblast-like and keratocyte-like cells. The motility factor of a keratocyte-like cell is larger than that of a fibroblast-like cell for different matrix rigidities.

cell adhesion. Our results suggest that the cell polarization shape complies with the principle of energy minimization. The influence of matrix rigidity has been considered in our energy model. In addition, a parameter called motility factor was suggested to depict the influence of matrix rigidity and cell polarization shape on the driving force of cell migration.

Our results show that there are two metastable cell shapes: disk-like non-polarized shape and spindle-like polarized shape of fibroblasts or crescent-like polarized shape of keratocytes. The polarized shape is regulated by several parameters, including polarization angle, tension of actin filament bundle at cell periphery, the length of cell tail, and the matrix rigidity. The total effect of these parameters leads to an energy-determined cell shape. Thus, our energy model describes the energy barrier of cell transformation from a non-polarized state to a polarized state [2,3].

We showed that the matrix rigidity plays a crucial role in regulating cell migration. On the one hand, matrix rigidity affects the cell polarization shape complying with the minimization of free energy. On the other hand, matrix rigidity affects the formation and de-adhesion of FACs, regulating the driving force of cell migration [50]. The biphasic dependence of both cell free energy and motility factor on matrix rigidity implies that the cell is in high-free-energy and low-motility states on a very soft or a very stiff matrix, while it is in low-free-energy and high-motility state for a matrix with intermediate rigidity. This result suggests that cells may regulate their migration behaviors by responding to the matrix rigidity.

To further understand the relationship between cell polarization and cell migration behaviors, we suggested a parameter called motility factor. This factor depicts the degree of coordination between the stability of cell adhesion at the cell front and the instability of cell adhesion at the cell rear. It has been shown that a relatively low force allows the growth and maturation of FACs that stabilizes the cell adhesion, while an excessively large force causes the disruption of cell adhesion [55,59,60]. It was also shown that the traction force increases with the distance from cell centroid [49]. And it was observed that the cell spreading area and focal adhesion area increase with increasing matrix rigidity. Thus, we can see that the motility factor can be co-influenced by matrix rigidity and cell shape. We obtained a biphasic relationship between motility factor and matrix rigidity, suggesting a biphasic feature of the driving force of cell migration. Furthermore, we showed that the motility factor of the keratocyte-like shape is much larger than that of the fibroblast-like one, implying a higher speed of the keratocyte than that of the fibroblast. Thus, the motility factor should be an appropriate parameter for a quantitative description of the driving force of cell migration.

Our predictions are broadly consistent with the experimental results. This study suggests that the cell polarization shape adopts the principle of energy minimization [2,44]. We showed that the larger the rigidity of the matrix, the higher the degree of cell polarization, which is consistent with experiments [3,20]. Our prediction of the biphasic dependence of motility factor on the rigidity of the matrix is consistent with experimental measurements of the dependence of cell migration speed on matrix rigidity [18,19]. Our results of the shape dependence of motility factor are consistent with the experiments showing that the velocity of a fibroblast (several tenth of micrometer per minute) is much lower than that of a keratocyte (a few tens of micrometer per minute) [58,61], and that the velocity is decreasing when a keratocyte occasionally possesses an abnormal shape with an elongated tail, as a fibroblast [5].

6. Conclusions

The cell polarization shape was studied by using an energy description, considering the influence of polarization angle, length of the cell tail, and matrix rigidity. The cell migration behavior is represented by a parameter called motility factor. We showed that the biphasic relationship between polarization angle and cell energy and that between tail length and cell

energy suggest that the cell shape adopts the principle of energy minimization for cell migration. Furthermore, the biphasic relationship between cell energy and matrix rigidity and that between motility factor and matrix rigidity imply that matrix rigidity plays a crucial role in cell shape and cell migration. The trends followed by cell free energy and motility factor with increasing matrix rigidity are opposite, and the value of the optimal matrix rigidity for a minimum cell energy is close to the one for a maximum motility factor. In addition, the fact that the motility factor of the keratocyte-like shape is higher than that of the fibroblast-like one suggests that the keratocyte-like shape is more favorable to fast cell migration, which is consistent with experiment. This study provides important insights into the relationship among cell polarization shape, matrix rigidity, and cell migration behavior.

Acknowledgements

References

[1] A. Mogilner, K. Keren, The shape of motile cells, Curr. Biol. 19 (2009) R762–R771.
[2] T. Mseka, J.R. Bamburg, L.P. Cramer, ADF/cofilin family proteins control formation of oriented actin-filament bundles in the cell body to trigger fibroblast polarization, J. Cell Sci. 120 (2007) 4332–4344.
[3] M. Prager-Khoutorsky, A. Lichtenstein, R. Krishnan, K. Rajendran, A. Mayo, Z. Kam, B. Geiger, A.D. Bershadsky, Fibroblast polarization is a matrix-rigidity-dependent process controlled by focal adhesion mechanosensing, Nat. Cell Biol. 13 (2011) 1457–1465.
[4] A.B. Verkhovsky, T.M. Svitkina, G.G. Borisy, Self-polarization and directional motility of cytoplasm, Curr. Biol. 9 (1999) 11–20.
[5] K. Burton, J.H. Park, D.L. Taylor, Keratocytes generate traction forces in two phases, Mol. Biol. Cell 10 (1999) 3745–3769.
[6] S. Munevar, Y.L. Wang, M. Dembo, Distinct roles of frontal and rear cell-substrate adhesions in fibroblast migration, Mol. Biol. Cell 12 (2001) 3947–3954.
[7] L.P. Cramer, Forming the cell rear first: breaking cell symmetry to trigger directed cell migration, Nat. Cell Biol. 12 (2010) 628–632.
[8] T. Mseka, L.P. Cramer, Actin depolymerization-based force retracts the cell rear in polarizing and migrating cells, Curr. Biol. 21 (2011) 2085–2091.
[9] Y.L. Wang, Reorganization of actin filament bundles in living fibroblasts, J. Cell Biol. 99 (1984) 1478–1485.
[10] A.B. Verkhovsky, T.M. Svitkina, G.G. Borisy, Myosin-II filament assemblies in the active lamella of fibroblasts—their morphogenesis and role in the formation of actin filament bundles, J. Cell Biol. 131 (1995) 989–1002.
[11] T.M. Svitkina, A.B. Verkhovsky, K.M. McQuade, G.G. Borisy, Analysis of the actin–myosin II system in fish epidermal keratocytes: mechanism of cell body translocation, J. Cell Biol. 139 (1997) 397–415.
[12] M.M. Kozlov, A. Mogilner, Model of polarization and bistability of cell fragments, Biophys. J. 93 (2007) 3811–3819.
[13] B. Vianay, J. Kaefer, E. Planus, M. Block, F. Graner, H. Guillou, Single cells spreading on a protein lattice adopt an energy minimizing shape, Phys. Rev. Lett. 105 (2010).
[14] Y. Ujihara, M. Nakamura, H. Miyazaki, S. Wada, Proposed spring network cell model based on a minimum energy concept, Ann. Biomed. Eng. 38 (2010) 1530–1538.
[15] X. Du, K. Doubrovinski, M. Osterfield, Self-organized cell motility from motor–filament interactions, Biophys. J. 102 (2012) 1738–1745.
[16] R. Bar-Ziv, T. Tlusty, E. Moses, S.A. Safran, A. Bershadsky, Pearling in cells: a clue to understanding cell shape, Proc. Natl. Acad. Sci. USA 96 (1999) 10140–10145.
[17] I.B. Bischofs, S.S. Schmidt, U.S. Schwarz, Effect of adhesion geometry and rigidity on cellular force distributions, Phys. Rev. Lett. 103 (2009) 048101.
[18] C.B. Khatiwala, S.R. Peyton, A.J. Putnam, Intrinsic mechanical properties of the extracellular matrix affect the behavior of pre-osteoblastic MC3T3-E1 cells, Am. J. Physiol., Cell Physiol. 290 (2006) C1640–C1650.
[19] S.R. Peyton, A.J. Putnam, Extracellular matrix rigidity governs smooth muscle cell motility in a biphasic fashion, J. Cell. Physiol. 204 (2005) 198–209.
[20] D.-H. Kim, K. Han, K. Gupta, K.W. Kwon, K.-Y. Suh, A. Levchenko, Mechanosensitivity of fibroblast cell shape and movement to anisotropic substratum topography gradients, Biomaterials 30 (2009) 5433–5444.
[21] A. Mogilner, G. Oster, Polymer motors: pushing out the front and pulling up the back, Curr. Biol. 13 (2003) R721–R733.
[22] A. Mogilner, Mathematics of cell motility: have we got its number? J. Math. Biol. 58 (2009) 105–134.
[23] I.V. Dokukina, M.E. Gracheva, A model of fibroblast motility on substrates with different rigidities, Biophys. J. 98 (2010) 2794–2803.
[24] A.S. Sarvestani, A model for cell motility on soft bio-adhesive substrates, J. Biomech. 44 (2011) 755–758.
[25] J. Lee, A. Ishihara, J.A. Theriot, K. Jacobson, Principles of locomotion for simple-shaped cells, Nature 362 (1993) 167–171.
[26] K. Keren, Z. Pincus, G.M. Allen, E.L. Barnhart, G. Marriott, A. Mogilner, J.A. Theriot, Mechanism of shape determination in motile cells, Nature 453 (2008) 475–480.
[27] E.L. Barnhart, K.-C. Lee, K. Keren, A. Mogilner, J.A. Theriot, An adhesion-dependent switch between mechanisms that determine motile cell shape, PLoS Biol. 9 (2011).
[28] M.S. Zand, G. Albrechtbuehler, What structures, besides adhesions, prevent spread cells from rounding up, Cell Motil. Cytoskelet. 13 (1989) 195–211.
[29] G.W. Fisher, P.A. Conrad, R.L. Debiasio, D.L. Taylor, Centripetal transport of cytoplasm, actin, and the cell surface in lamellipodia of fibroblasts, Cell Motil. Cytoskelet. 11 (1988) 235–247.
[30] R. Rid, N. Schiefermeier, I. Grigoriev, J.V. Small, I. Kaverina, The last but not the least: the origin and significance of trailing adhesions in fibroblastic cells, Cell Motil. Cytoskelet. 61 (2005) 161–171.
[31] L. Lu, Y. Feng, W.J. Hucker, S.J. Oswald, G.D. Longmore, F.C.P. Yin, Actin stress fiber pre-extension in human aortic endothelial cells, Cell Motil. Cytoskelet. 65 (2008) 281–294.
[32] B. Ji, G. Bao, Cell and molecular biomechanics: perspectives and challenges, Acta Mech. Solida Sin. 24 (2011) 27–51.
[33] Y. Zhong, D. Kong, L. Dai, B. Ji, Frequency-dependent focal adhesion instability and cell reorientation under cyclic substrate stretching, Cell. Mol. Bioeng. 4 (2011) 442–456.
[34] R. Paul, P. Heil, J.P. Spatz, U.S. Schwarz, Propagation of mechanical stress through the actin cytoskeleton toward focal adhesions: model and experiment, Biophys. J. 94 (2008) 1470–1482.
[35] S. Deguchi, T. Ohashi, M. Sato, Tensile properties of single stress fibers isolated from cultured vascular smooth muscle cells, J. Biomech. 39 (2006) 2603–2610.
[36] M. They, A. Pein, E. Dressaire, Y. Chen, M. Bornens, Cell distribution of stress fibres in response to the geometry of the adhesive environment, Cell Motil. Cytoskelet. 63 (2006) 341–355.

[37] I.B. Bischofs, F. Klein, D. Lehnert, M. Bastmeyer, U.S. Schwarz, Filamentous network mechanics and active contractility determine cell and tissue shape, Biophys. J. 95 (7) (2008) 3488–3496, http://dx.doi.org/10.1529/biophysj.108.134296.
[38] K. Kendall, The adhesion and surface energy of elastic solids, J. Phys. D, Appl. Phys. 4 (1971) 1186–1195.
[39] X. Peng, J. Huang, C. Xiong, J. Fang, Cell adhesion nucleation regulated by substrate stiffness: a Monte Carlo study, J. Biomech. 45 (2012) 116–122.
[40] G.A. Dunn, D. Zicha, Dynamics of fibroblast spreading, J. Cell Sci. 108 (1995) 1239–1249.
[41] J.W. Dai, M.P. Sheetz, X.D. Wan, C.E. Morris, Membrane tension in swelling and shrinking molluscan neurons, J. Neurosci. 18 (1998) 6681–6692.
[42] W. Helfrich, Elasticity and Thermal Undulations of Fluid Films of Amphiphiles, Elsevier, North-Holland, Amsterdam, The Netherlands, 1990.
[43] J. Lee, K. Jacobson, The composition and dynamics of cell-substratum adhesions in locomoting fish keratocytes, J. Cell Sci. 110 (1997) 2833–2844.
[44] K.A. Beningo, M. Dembo, I. Kaverina, J.V. Small, Y.-l. Wang, Nascent focal adhesions are responsible for the generation of strong propulsive forces in migrating fibroblasts, J. Cell Biol. 153 (2001) 881–888.
[45] B. Ji, B. Huo, Probing the mechanosensitivity in cell adhesion and migration: experiments and modeling, Acta Mech. Sin. 29 (2013) 469–484.
[46] J.L. Tan, J. Tien, D.M. Pirone, D.S. Gray, K. Bhadriraju, C.S. Chen, From the cover: cells lying on a bed of microneedles: an approach to isolate mechanical force, Proc. Natl. Acad. Sci. 100 (2003) 1484–1489.
[47] A.D. Bershadsky, N.Q. Balaban, B. Geiger, Adhesion-dependent cell mechanosensitivity, Annu. Rev. Cell Dev. Biol. 19 (2003) 677–695.
[48] N.Q. Balaban, U.S. Schwarz, D. Riveline, P. Goichberg, G. Tzur, I. Sabanay, D. Mahalu, S.A. Safran, A. Bershadsky, L. Addadi, B. Geiger, Force and focal adhesion assembly: a close relationship studied using elastic micropatterned substrates, Nat. Cell Biol. 3 (2001) 466–472.
[49] C.A. Lemmon, L.H. Romer, A predictive model of cell traction forces based on cell geometry, Biophys. J. 99 (2010) L78–L80.
[50] Y. Zhong, B. Ji, Impact of cell shape on cell migration behavior on elastic substrate, Biofabrication 5 (2013) 015011.
[51] A.D. Rape, W.-h. Guo, Y.-l. Wang, The regulation of traction force in relation to cell shape and focal adhesions, Biomaterials 32 (2011) 2043–2051.
[52] J. Stricker, Y. Aratyn-Schaus, P.W. Oakes, M.L. Gardel, Spatiotemporal constraints on the force-dependent growth of focal adhesions, Biophys. J. 100 (2011) 2883–2893.
[53] Y. Zhong, S. He, B. Ji, Mechanics in mechanosensitivity of cell adhesion and its roles in cell migration, Int. J. Comput. Mater. Sci. Eng. 1 (2012) 1250032.
[54] D.R.B. Aroush, R. Zaidel-Bar, A.D. Bershadsky, H.D. Wagner, Temporal evolution of cell focal adhesions: experimental observations and shear stress profiles, Soft Matter 4 (2008) 2410–2417.
[55] D. Kong, B.H. Ji, L.H. Dai, Stabilizing to disruptive transition of focal adhesion response to mechanical forces, J. Biomech. 43 (2010) 2524–2529.
[56] C.G. Galbraith, K.M. Yamada, M.P. Sheetz, The relationship between force and focal complex development, J. Cell Biol. 159 (2002) 695–705.
[57] J.M. Goffin, P. Pittet, G. Csucs, J.W. Lussi, J.J. Meister, B. Hinz, Focal adhesion size controls tension-dependent recruitment of alpha-smooth muscle actin to stress fibers, J. Cell Biol. 172 (2006) 259–268.
[58] C.-M. Lo, H.-B. Wang, M. Dembo, Y.-l. Wang, Cell movement is guided by the rigidity of the substrate, Biophys. J. 79 (2000) 144–152.
[59] D. Kong, B. Ji, L. Dai, Stability of adhesion clusters and cell reorientation under lateral cyclic tension, Biophys. J. 95 (2008) 4034–4044.
[60] D. Kong, B. Ji, L. Dai, Nonlinear mechanical modeling of cell adhesion, J. Theor. Biol. 250 (2008) 75–84.
[61] C. Jurado, J.R. Haserick, J. Lee, Slipping or gripping? Fluorescent speckle microscopy in fish keratocytes reveals two different mechanisms for generating a retrograde flow of actin, Mol. Biol. Cell 16 (2005) 507–518.
[62] V.C. Abraham, V. Krishnamurthi, D.L. Taylor, F. Lanni, The actin-based nanomachine at the leading edge of migrating cells, Biophys. J. 77 (1999) 1721–1732.
[63] R.J. Pelham, Y.L. Wang, Cell locomotion and focal adhesions are regulated by substrate flexibility, Proc. Natl. Acad. Sci. USA 94 (1997) 13661–13665.
[64] J. Solon, I. Levental, K. Sengupta, P.C. Georges, P.A. Janmey, Fibroblast adaptation and stiffness matching to soft elastic substrates, Biophys. J. 93 (2007) 4453–4461.